

- at $X = -75$ km and $X = 90$ km.
9. The heterogeneity within the Franciscan accretionary terranes [J. A. Goff and A. R. Levander, *J. Geophys. Res.* **101**, 8489 (1996)] is not resolved. Upper crustal velocities change (by 0.1 to 0.2 km/s) across the SAF, representing the difference between an old accretionary wedge and terranes involved in subduction until 2 to 3 Ma.
 10. Apparent lower-crustal offsets in reflection data could be caused by basins near the fault zones or by changes in crustal velocities across the faults. However, to explain travel-time anomalies in wide-angle reflections and refractions by shallow structure would require basins offset from the faults, because these arrivals travel laterally through the crust. The simplest explanation for all the observations is that the anomalies arise near the base of the crust.
 11. The kinked velocity model has a Moho slope of 10° west of the surface trace of the SAF and a Moho slope of 5° east of the SAF surface trace, so that the kink describes the point where the slope changes. The depths of the Moho at the endpoints of the slopes are: 12 km at $X = -77$ km, 21 km at $X = -20$ km, and 29 km at $X = 80$ km.
 12. The rms travel-time misfit for 3100 lower crustal and upper mantle picks is 164 ms for the stepped model, with a reduced χ^2 of 1.4, compared with 186 ms and 1.9 for the kinked model. Most of the additional error arises in the onshore-offshore P_n phase.
 13. Depth migration focuses reflected energy at the reflector location [W. A. Schneider, *Geophysics* **43**, 49, (1978)]. It is routinely applied to near-vertical data; our application to onshore-offshore data links marine reflection data and a single-fold land section. The different data types cause changes in appearance of the section at $X = -30$ km and $X = 1$ km on the profile.
 14. K. P. Furlong, W. D. Hugo, G. Zandt, *J. Geophys. Res.* **94**, 3100 (1989).
 15. T. M. Brocher *et al.*, *Science* **265**, 1436 (1994).
 16. W. S. Holbrook, T. M. Brocher, U. S. ten Brink, J. A. Hole, *J. Geophys. Res.* **101**, 22311 (1996).
 17. A. S. Meltzer and A. R. Levander, *ibid.* **96**, 6475 (1991); J. M. Howie, K. C. Miller, W. U. Savage, *ibid.* **98**, 8173 (1993); K. C. Miller, J. M. Howie, S. D. Ruppert, *ibid.* **97**, 19961 (1992); C. F. Lafond and A. Levander, *ibid.* **100**, 22231 (1995).
 18. H. M. Kelsey and G. A. Carver, *ibid.* **93**, 4797 (1988); D. A. Castillo and W. L. Ellsworth, *ibid.* **98**, 6543 (1993).
 19. B. M. Page and T. M. Brocher, *Geology* **21**, 635 (1993).
 20. R. G. Bohannon and T. Parsons, *Geol. Soc. Am. Bull.* **107**, 937 (1995).
 21. R. C. Jachens, A. Griscorn, C. W. Roberts, *J. Geophys. Res.* **100**, 12769 (1995).
 22. This is within the limits of DeMets *et al.* (1) but is higher than the 95% limits of -1 to $+5$ mm/year for present shortening of Argus and Gordon (1).
 23. A. J. Calvert, *Can. Jour. Earth Sci.* **33**, 1294 (1996).
 24. S. W. Smith, J. S. Knapp, R. C. McPherson, *J. Geophys. Res.* **98**, 8153 (1993).
 25. Assumptions that adiabatic upwelling of mantle into the slab window extends to the base of the accretionary rocks and fills the space vacated by the Gorda slab allow us to use published calculations [D. McKenzie and M. J. Bickle, *J. Petrol.* **29**, 625 (1988)] to estimate the melt generated. For 1300°C mantle, this is about 2 km, and to explain the thickness of the LCL would require temperatures 100° to 150°C higher. Petrologic consequences of higher mantle temperatures are discussed by McKenzie and Bickle.
 26. To match the wide-angle velocity structure and near-vertical reflectivity requires thin bodies with too great a material contrast for a solid-solid contact so that fluids must be present. Our interpretation that these represent melt intrusions is based on the tectonic setting [A. Levander *et al.*, in preparation].
 27. We are grateful to the many people who assisted in the 1993 and 1994 field programs, the IRIS-PASSCAL program, and Lamont-Doherty Earth Observatory. Earthquake locations were obtained from the northern California earthquake network operated by the U.S. Geological Survey and the

Seismographic Station of U.C. Berkeley. The seismic data are available through the IRIS Data Management Center. We thank other members of the MTJ seismic experiment working group and R. G. Gordon for comments on this manuscript. This study

was funded by National Science Foundation Continental Dynamics program grants EAR-9218968 and EAR-952693.

16 July 1997; accepted 3 October 1997

Synthesis of Nanoparticles and Nanotubes with Well-Separated Layers of Boron Nitride and Carbon

K. Suenaga, C. Colliex,* N. Demoncey, A. Loiseau, H. Pascard, F. Willaime

Polyhedral and tubular graphitic nanoparticles made of carbon layers and boron nitride (BN) layers have been synthesized. These particles were observed in the soot collected on the anode deposit formed by arcing a hafnium diboride rod with graphite in a nitrogen atmosphere. Elemental profiles with subnanometer-scale resolution revealed a strong phase separation between BN layers and carbon layers along the radial direction. Most of these tubes have a sandwich structure with carbon layers both in the center and at the periphery, separated by a few BN layers. This structure provides insight into the atomistic mechanism of nanotube growth in the boron-carbon-nitrogen ternary system and may lead to the creation of nanostructured electronic devices relying on the controlled production of heteroatomic nanotubes.

The family of graphitic nanoparticles with tubular or spherical shape has expanded rapidly since the discovery of carbon nanotubes (1) and carbon onions (2), which consist of a few concentric cylindrical or spherical carbon layers. Their pure BN analogs have now been successfully synthesized (3–5). The electronic properties of these nanoparticles open up new possibilities for making nanoscale electronic devices, in particular from the tubular form (6). On the basis of theoretical predictions suggesting that the electronic properties of carbon nanotubes will range from metallic to semiconducting with a small gap, depending on the tube diameter and chirality (7), the idea of making electronic switches by connecting pure carbon nanotubes was first proposed (8). This concept was recently generalized to heterojunctions between

$\text{B}_x\text{C}_y\text{N}_z$ nanotubes with different chemical compositions (9). The advantage of such nanotubes is that their electronic properties are primarily determined by composition and are thus relatively easy to control. For example, BN nanotubes are predicted to be semiconducting, with a wide gap close to the 5.8-eV gap of bulk hexagonal BN (10). In this context, uniformly doped carbon nanotubes, as well as nanotubes with other chemical compositions such as BC_2N or BC_3 (11), would be interesting for their electronic properties. However, their synthesis has not yet been achieved in a controllable fashion, although portions of such tubes among a majority of pure carbon tubes have been reported (12–14).

Here, we report the synthesis of a soot containing polyhedral and tubular nanoparticles that consist of well-separated BN layers and carbon layers. In previous arc-discharge syntheses of B-C-N tubes, it was shown that when the anode contains carbon, the graphitic products contain mostly carbon (12–14). Either a low doping by B and N (less than 2%) or very low concentrations of B-rich or BN-rich nanotubes have been reported. In our study, this drawback was overcome by modifying the original geometry used to produce pure BN tubes (5). A graphite cathode—used instead of the original HfB_2 rod—is arced with an HfB_2 anode in a nitrogen atmosphere. In the present configuration, the three constituents have different sources: the anode for boron, the cathode (which slightly vaporizes in the present case) for carbon, and the

K. Suenaga, Laboratoire de Physique des Solides, URA 002, Université de Paris-Sud, Bât. 510, 91405 Orsay, France.

C. Colliex, Laboratoire de Physique des Solides, URA 002, Université de Paris-Sud, Bât. 510, 91405 Orsay, France, and Laboratoire Aimé Cotton, UPR 3321, Campus d'Orsay, Bât. 505, 91405 Orsay, France.

N. Demoncey, Laboratoire des Solides Irradiés, CEA-CNRS, Ecole Polytechnique, 91128 Palaiseau Cédex, France, and Laboratoire de Physique des Solides, Office National d'Etudes et de Recherches Aéronautiques, BP 72, 92322 Châtillon, France.

A. Loiseau, Laboratoire de Physique des Solides, Office National d'Etudes et de Recherches Aéronautiques, BP 72, 92322 Châtillon, France.

H. Pascard, Laboratoire des Solides Irradiés, CEA-CNRS, Ecole Polytechnique, 91128 Palaiseau, France. F. Willaime, Section de Recherches de Métallurgie Physique, CEA/Saclay, 91191 Gif-sur-Yvette, France.

*To whom correspondence should be addressed.

chamber atmosphere for nitrogen (15). In addition, hafnium present in the plasma may be acting as a catalyst. This geometry allows the production of nanoparticles with interesting chemical structures, provides insights into the complex processes taking place in the formation of nanotubes in an arc discharge, and may lead to the controlled production of nanotube heterojunctions. To determine the chemical composition of the present structures at a scale close to the 0.34-nm interlayer spacing, we used quantitative electron energy loss spectroscopy (EELS) with high spatial resolution (16). This technique is well suited to characterize the relevant chemistry and electronic structure of the present hybrid BN-C nanostructures. The following results concentrate on the anode deposit.

The dominant products are metallic hafnium boride nanoparticles, typically 5 to 20 nm in diameter, encapsulated in

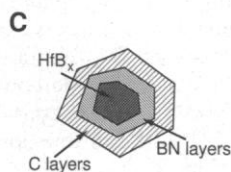
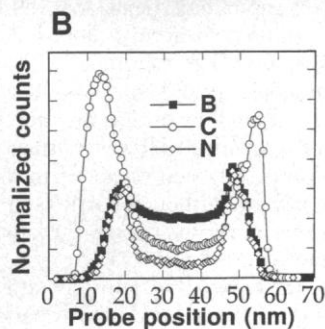
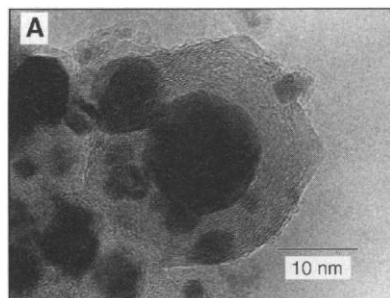


Fig. 1. (A) Transmission electron microscope (TEM) image of a polyhedral nanoparticle with a metallic hafnium boride core (darkest contrast) encapsulated by graphitic layers. (B) Elemental profiles of B, C, and N across a similar but larger particle, showing BN inner shells and carbon outer shells. Both the BN shell and the hafnium boride particle contribute to the B counts at the center point. (C) Schematic cross-section representation of the double-coated nanoparticle structure. The metallic particle is covered with about 15 layers of BN and 28 layers of carbon.

polyhedral concentric graphitic shells with 10 to 50 layers (Fig. 1A). The elemental profiles of B, C, and N (17) (Fig. 1B), obtained by scanning the electron probe across such a particle, demonstrate unambiguously that the outer shells are pure carbon layers and that the inner shells are BN-rich layers, probably pure BN. The correlation between the N profile and the B profile—except in the region where the probe includes the hafnium boride particle—shows that B and N are equiatomic in the graphitic layers. This three-shell nanoparticle therefore has a metallic core (hafnium boride) with a first insulating envelope (graphitic BN) and a second (potentially) semimetallic envelope (graphitic carbon) (Fig. 1C). Similar particles with an empty core were also found.

Particles with a nanotubular shape, typically 4 to 12 nm in outer diameter, were also observed (Fig. 2A). The layers of these tubes have various chemical compositions. Besides the atypical case of pure BN tubes, all tubes were found to have well-separated BN layers and carbon layers. Two types of tubes were observed: one where the inner BN layers are coated by carbon layers (as in the case of the polyhedral particles described above), and another, which is dominant and more intriguing, with a sandwich configuration.

From the concentration profiles taken across such a tube, the presence in the C profile of four maxima and two minima coinciding with the two maxima of the B and N profiles clearly indicates an alternating C-rich–BN-rich–C-rich geometry (Fig. 2B). These profiles were simulated for various distributions of layers with different chemical compositions (Fig. 2C). The best agreement with experiment was obtained in this case for a 14-layer tube, 12 nm in external diameter, formed with three inner layers of graphitic carbon covered by six (BN)_xC_{2y} layers (with $y/x \approx 0.05 \pm 0.05$) and five outer carbon layers (Fig. 2D). The fine structures of the B and C K-edges (Fig. 2E) confirm the graphitic network with the sp^2 -type configuration. Moreover, the evolution of the weight ratio between the π^* and σ^* peaks as the probe scans from the edge to the center is characteristic of a cylindrical structure (18), where the orientation of the electron beam with respect to the graphitic layers varies continuously from parallel to perpendicular. Similar observations were made for other tubes.

These results show that hybrid BN-C nanoparticles can be produced in both polyhedral and tubular forms. The average carbon content within the graphitic layers ranges from 20 to 80 atomic %, and no preferred stoichiometry (such as BC₂N) is

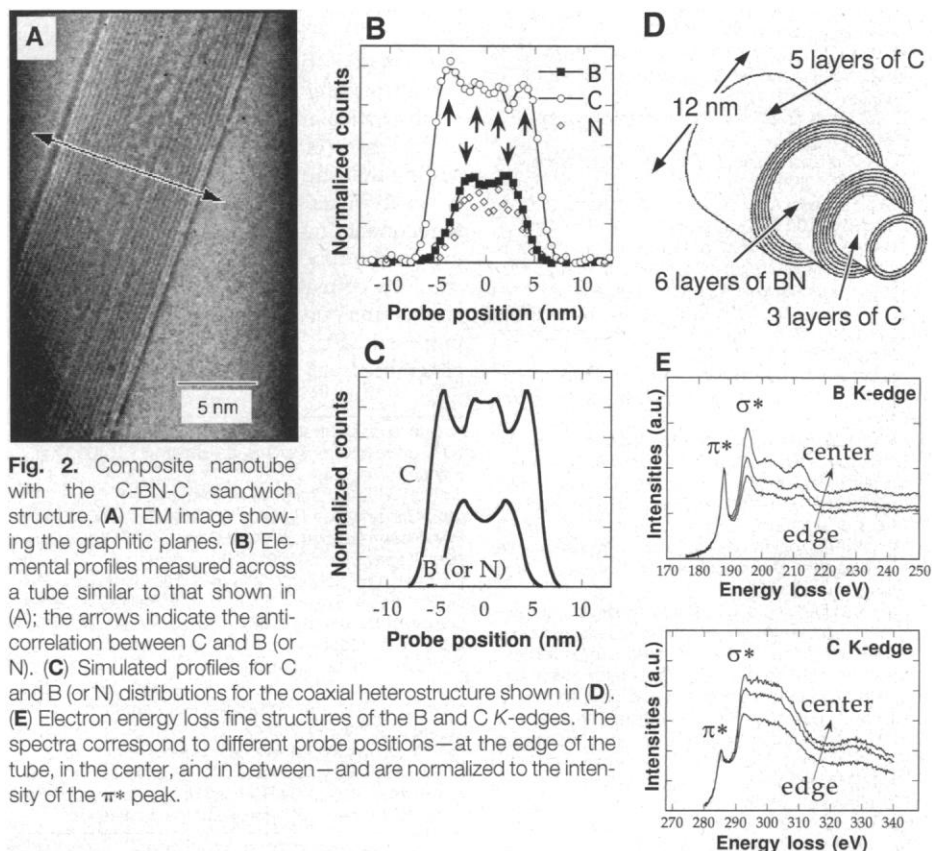


Fig. 2. Composite nanotube with the C-BN-C sandwich structure. (A) TEM image showing the graphitic planes. (B) Elemental profiles measured across a tube similar to that shown in (A); the arrows indicate the anti-correlation between C and B (or N). (C) Simulated profiles for C and B (or N) distributions for the coaxial heterostructure shown in (D). (E) Electron energy loss fine structures of the B and C K-edges. The spectra correspond to different probe positions—at the edge of the tube, in the center, and in between—and are normalized to the intensity of the π^* peak.

observed. The common feature for all the nanoparticles present in the soot is the strong phase separation between chemical species (B and N on one side and C on the other side). Therefore, it is realistic to propose nanotube-based devices compatible with this phase separation, such as axial BN-C heterojunctions or superlattices (10), whereas the production of homogeneous nanotubes with an ordered BC₂N structure (11) appears more difficult to control, at least under arc-discharge conditions.

The clear phase separation observed between BN layers and C layers raises the question of the growth mechanism itself. A segregation process taking place by diffusion between layers after the particles are formed can be ruled out because of the very slow interlayer diffusion rates. A workable hypothesis is that BN particles grow first and then go through a carbon-rich region of the plasma, leading to a carbon coating on the surface of all particles. For the C-BN-C sandwich geometry observed in most tubes, it must then be assumed that the coating is also efficient for the inner surface of the tube and that it occurs by diffusion of carbon atoms from the open-ended tip of the tube. A similar scenario has been reported for the filling and coating of carbon nanotubes by molten V₂O₅ (19). The inner coating of the polyhedral nanoparticles is prevented by their close-shelled nature. In the case of the tubes, another scenario can be envisioned in which the BN shells and the carbon shells grow simultaneously. Ab initio molecular dynamics simulations of the growth mechanism of a bilayer tube have shown that lip-lip interactions are important and that adjacent layers are connected by bridges saturating the dangling bonds (20). Fast diffusion processes leading to phase separation could take place within these bridges.

The sandwich C-BN-C geometry found for some tubes closely resembles the metal-insulator-metal geometry of the memory device proposed for nanotube applications (6) as well as that of a coaxial nanocable. The key to producing mixed nanotubes while avoiding the dominant formation of carbon tubes is to control the vaporization of carbon. Taking advantage of the natural phase separation between BN and C under arc-discharge conditions should make it possible to achieve the controlled production of nanotubes in which BN and C are alternated either between layers or within the layers. Measuring the electrical properties of these composite tubes—as was recently done in the case of pure carbon tubes, including single-wall tubes (21)—is of particular interest.

REFERENCES AND NOTES

1. S. Iijima, *Nature* **354**, 54 (1991).
2. D. Ugarte, *ibid.* **359**, 707 (1992).
3. L. Boulanger, F. Willaime, M. Cauchetier, in *Proceedings of the 13th International Conference on Electron Microscopy*, vol. IIIA, B. Jouffrey and C. Colliex, Eds. (Editions de Physique, Paris, 1994), pp. 315–316; L. Boulanger, B. Andriot, M. Cauchetier, F. Willaime, *Chem. Phys. Lett.* **234**, 227 (1995); F. Banhart, M. Zwanger, H. J. Muhr, *ibid.* **231**, 98 (1994).
4. N. G. Chopra *et al.*, *Science* **269**, 966 (1995); M. Terrones *et al.*, *Chem. Phys. Lett.* **259**, 568 (1996).
5. A. Loiseau, F. Willaime, N. Demoncey, G. Hug, H. Pascard, *Phys. Rev. Lett.* **76**, 4737 (1996).
6. M. S. Dresselhaus, G. Dresselhaus, P. C. Eklund, *Science of Fullerenes and Carbon Nanotubes* (Academic Press, London, 1996), p. 903.
7. N. Hamada, S. Sawada, A. Oshiyama, *Phys. Rev. Lett.* **68**, 1579 (1992); R. Saito, M. Fujita, G. Dresselhaus, M. S. Dresselhaus, *Phys. Rev. B* **46**, 1804 (1992).
8. P. Lambin, A. Fonseca, J. P. Vigneron, J. B. Nagy, A. A. Lucas, *Chem. Phys. Lett.* **245**, 85 (1995); R. Saito, G. Dresselhaus, M. S. Dresselhaus, *Phys. Rev. B* **53**, 2044 (1996); L. Chico, L. X. Benedict, S. G. Louie, M. L. Cohen, *Phys. Rev. Lett.* **76**, 971 (1996).
9. X. Blase, J.-C. Charlier, A. De Vita, R. Car, *Appl. Phys. Lett.* **70**, 197 (1997); E. G. Gal'pern, V. V. Pinyaskin, I. V. Stankevish, L. A. Chernozatonskii, *J. Phys. Chem. B* **101**, 705 (1997).
10. X. Blase, A. Rubio, S. G. Louie, M. L. Cohen, *Europhys. Lett.* **28**, 335 (1994).
11. Y. Miyamoto, A. Rubio, M. L. Cohen, S. G. Louie, *Phys. Rev. B* **50**, 18360 (1994); *ibid.*, p. 4976.
12. O. Stephan *et al.*, *Science* **266**, 1683 (1994).
13. Z. Weng-Sieh *et al.*, *Phys. Rev. B* **51**, 11229 (1995).
14. Ph. Redlich *et al.*, *Chem. Phys. Lett.* **260**, 465 (1996).
15. Taking advantage of the gas ambient as a constituent has led to the successful synthesis of BN tubes (5) and doping of carbon tubes (12) in arc methods. It may be possible to control the chemical composition of the tubes by monitoring the gas composition in the chamber.
16. A scanning transmission electron microscope (STEM VG-HB501) equipped with a parallel detector (Gatan PEELS 666) was operated at 100 kV. See, for example, C. Colliex, *J. Electron Microsc.* **45**, 44 (1996).
17. All the K-edge weights are normalized by hydrogenic cross section and the elastic peak for each element; therefore, the profiles are proportional to the numbers of selected atoms. The smallest probe (0.5 nm) was used. Acquisition time for the EELS was reduced to 1 s to prevent beam-induced effects at the cost of a reduction of signal-to-noise ratio in N K-edge counts in some cases. For details, see R. F. Egerton, *EELS in the Electron Microscope* (Plenum, New York, ed. 2, 1996); C. Colliex, in *EELS in Materials Science*, M. M. Disko, C. C. Ahn, B. Fultz, Eds. (TMS, Minerals, Metals, Materials Society, Warrendale, PA, 1992), pp. 86–106.
18. O. Stephan, P. M. Ajayan, C. Colliex, F. Cyrot-Lackmann, E. Sandre, *Phys. Rev. B* **53**, 13824 (1996).
19. P. M. Ajayan, O. Stephan, Ph. Redlich, C. Colliex, *Nature* **375**, 564 (1995).
20. J.-C. Charlier, A. De Vita, X. Blase, R. Car, *Science* **275**, 646 (1997).
21. S. J. Tans *et al.*, *Nature* **386**, 474 (1997).
22. We thank X. Deschanel (CEA/Saclay) for providing hafnium diboride rods. Partially supported by NEDO international joint research grant "Novel Nanotubular Materials: Production, Characterization and Properties."

7 July 1997; accepted 9 September 1997

Nanotubule-Based Molecular-Filtration Membranes

Kshama B. Jirage, John C. Hulthen, Charles R. Martin*

Polymeric membranes that contain a collection of monodisperse gold nanotubules, with inside diameters of molecular dimensions (less than 1 nanometer), were used in a simple membrane-permeation experiment to cleanly separate small molecules on the basis of molecular size. For example, when such a membrane was presented with an aqueous feed solution containing pyridine (molecular weight 79) and quinine (molecular weight 324), only the smaller pyridine molecule was transported through the nanotubules and into a receiver solution on the other side of the membrane.

Membrane-based chemical separations are potentially more economical and easier to implement than competing separations technologies, but membranes with higher transport selectivities are required (1–5). Chemical features of the membrane, and of the molecule to be selectively transported, that can be exploited to enhance transport selectivity include charge, chemical interactions, and molecular size. The ideal approach for implementing molecular size-based transport selectivity would be to de-

sign a synthetic membrane that has a collection of monodisperse nanopores, of molecular dimensions, that span the complete thickness of the membrane. If this could be accomplished, one could envision general "molecular filters" that could be used in a simple membrane-permeation experiment to cleanly separate small molecules on the basis of size. We describe such membranes here.

This idea of using membranes to filter molecules on the basis of size is not without precedent. Dialysis is used routinely to separate low-molecular weight species from macromolecules (6). In addition, nanofiltration membranes are known for certain small-molecule separations (such as water

Department of Chemistry, Colorado State University, Fort Collins, CO 80523, USA.

*To whom correspondence should be addressed at cmartin@lamar.colostate.edu